

## ANALYTICAL MODELING OF ELASTOMERIC ISOLATION BEARINGS UNDER SEVERE AXIAL LOAD AND SHEAR DEFORMATIONS

S. Yamamoto<sup>1</sup>, M. Kikuchi<sup>2</sup>, M. Ueda<sup>3</sup> and I.D. Aiken<sup>4</sup>

<sup>1</sup> Graduate Student, Graduate School of Engineering, Hokkaido University, Japan.

<sup>2</sup> Associate Professor, Graduate School of Engineering, Hokkaido University, Japan.

<sup>3</sup> Professor, Graduate School of Engineering, Hokkaido University, Japan.

<sup>4</sup> Principal, Seismic Isolation Engineering Inc., USA.

Email: sachi615@eng.hokudai.ac.jp

### ABSTRACT :

This paper presents a new analytical model for elastomeric seismic isolation bearings. Elastomeric isolation bearings exhibit stiffening or buckling behavior influenced by the applied compressive stress under large shear deformations. The isolator properties depend on the interaction between the horizontal and vertical forces on the isolator. A new analytical model has been developed to predict the behavior of elastomeric isolators under high vertical loads and large shear deformations. The model includes the interaction between horizontal and vertical forces as well as the nonlinear hysteresis characteristics of elastomeric isolators at large shear deformations. The model captures isolator behavior due to varying vertical load, which is a necessary feature to accurately predict the influence of building overturning on isolation system response in an earthquake. To validate the model, simulation analyses of cyclic shear tests of lead-rubber bearings under constant and varying vertical load and cyclic shear deformations were conducted. The hysteresis loops obtained from the tests under constant compressive stress exhibited shear stiffening behavior for low compressive stress, with deterioration of horizontal stiffness under high compressive stress. The varying vertical load test hysteresis loops were not symmetric, rather they showed both stiffening behavior and a deterioration of horizontal stiffness depend on the level of vertical load. These test results show that compressive load strongly influences the shape of the shear hysteresis loops. The results of the analyses using the new model show very good agreement with both the constant and varying vertical load experimental results.

**KEYWORDS:** seismic isolation, base isolation, elastomeric isolation bearing, large deformation, axial load, nonlinear hysteresis model

### 1. INTRODUCTION

Seismic isolation is the most effective technology for protecting structures from the damaging effects of earthquakes. It has been extensively used worldwide over the last three decades. The widespread use of seismic isolation has necessitated better understanding of some of the more complex aspects of isolation device behavior, such as under large shear deformations or high compressive stresses. Elastomeric isolation bearings exhibit stiffening or buckling behavior, influenced by the imposed compressive stress at large shear deformations. The change in shear stiffness due to high compressive stress is an important behavior to consider for elastomeric bearings when isolated buildings experience extreme earthquake shaking. The properties of seismic isolation devices depend upon the interaction between shear and vertical forces acting on the isolator. The actual hysteretic behavior of an isolation bearing under a structure subjected to severe earthquake shaking is influenced by the variation of vertical load on the isolator due to overturning forces. In addition to the shear-axial interaction, elastomeric isolation bearings exhibit nonlinear behavior at large shear displacements. To predict the response of isolated structures under large bearing shear displacements, an analytical method that accounts for both nonlinear bearing behavior in large shear deformations and the effect of varying vertical load on bearing properties is needed. In this paper, a new analytical model for elastomeric bearings with these capabilities is proposed. The new model includes the interaction between shear and axial forces as a function of

varying vertical load on a bearing during earthquake loading.

## 2. A NEW MECHANICAL MODEL FOR ELASTOMERIC BEARINGS

Figure 1 shows the proposed new mechanical model to incorporate interaction between shear and axial forces as a function of varying vertical load. The model is developed based on the geometrical relationships of the Koh-Kelly model [1]. The model comprises shear and axial springs, and two series of axial springs at the top and bottom boundaries. Each spring in the series of axial springs represents an individual strip of the bearing cross-sectional area. The rigid columns, which represent the height of the bearing, are combined between the series of axial springs and the mid-height shear and the axial springs. Each spring in the model is a uniaxial, nonlinear spring. When this collection of springs is combined in the model, the nonlinear, interaction behavior is achieved. The nodes,  $a$ ,  $m$ ,  $n$  and  $b$ , in Figure 1 are the points where the components of the mechanical model inter-connect. The nodes,  $a$  and  $b$ , have displacements in three directions (horizontal, vertical and rotational) and the nodes,  $m$  and  $n$ , have displacements in two directions (vertical and rotational). The node pairs  $a$  and  $m$ , and  $b$  and  $n$ , are spatially coincident. The horizontal displacements of the nodes,  $m$  and  $n$ , are equal to those of the nodes,  $a$  and  $b$ , respectively. The forces and displacements on the model are also shown in Figure 1.

As the incremental forces on nodes  $a$  and  $m$  are the sums of the incremental restoring forces on the series of axial springs between  $a$  and  $m$ , the force-displacement relationship on nodes  $a$  and  $m$  may be written as follows:

$$\begin{Bmatrix} \Delta f_{va} \\ \Delta m_a \\ \Delta f_{vm} \\ \Delta m_m \end{Bmatrix} = \begin{bmatrix} {}_1k_a & {}_2k_a & -{}_1k_a & -{}_2k_a \\ & {}_3k_a & -{}_2k_a & -{}_3k_a \\ & & {}_1k_a & {}_2k_a \\ \text{Symm.} & & & {}_3k_a \end{bmatrix} \begin{Bmatrix} \Delta v_a \\ \Delta \theta_a \\ \Delta v_m \\ \Delta \theta_m \end{Bmatrix} \quad (2.1)$$

where

$$\begin{aligned} {}_1k_a &= \sum_i K_{Na} \\ {}_2k_a &= \sum_i K_{Na} i l_a \\ {}_3k_a &= \sum_i K_{Na} i l_a^2 \end{aligned}$$

where  ${}_iK_{Na}$  is the stiffness of the  $i$ -th axial spring located between nodes  $a$  and  $m$ , and  ${}_i l_a$  is the length between the  $i$ -th spring and the center of the series of axial springs, which represents the distance from the centroid of the  $i$ -th strip to the center of the cross-sectional area of the bearing. The incremental vertical force and bending moment on nodes  $n$  and  $b$  are the sums of restoring forces on the series of axial springs between  $n$  and  $b$ . The force-displacement relationship on nodes  $n$  and  $b$  may be also written in the same way as Eqn. 2.1.

Taking the geometrical relationships of the deformations, the force-equilibrium condition and P- $\Delta$  effect into account gives the force-displacement relationship on the interior nodes,  $m$  and  $n$ :

$$\begin{Bmatrix} \Delta f_{ha} \\ \Delta f_{vm} \\ \Delta m_m \\ \Delta f_{hb} \\ \Delta f_{vn} \\ \Delta m_n \end{Bmatrix} = \begin{bmatrix} {}_1k_{mn} & -{}_4k_{mn} & -{}_6k_{mn} & -{}_3k_{mn} & {}_4k_{mn} & -{}_6k_{mn} \\ & {}_8k_{mn} & {}_9k_{mn} & {}_5k_{mn} & -{}_8k_{mn} & {}_9k_{mn} \\ & & {}_{10}k_{mn} & {}_7k_{mn} & -{}_9k_{mn} & {}_{11}k_{mn} \\ & & & {}_2k_{mn} & -{}_5k_{mn} & {}_7k_{mn} \\ \text{Symm.} & & & & {}_8k_{mn} & -{}_9k_{mn} \\ & & & & & {}_{10}k_{mn} \end{bmatrix} \begin{Bmatrix} \Delta u_a \\ \Delta v_m \\ \Delta \theta_m \\ \Delta u_b \\ \Delta v_n \\ \Delta \theta_n \end{Bmatrix} \quad (2.2)$$

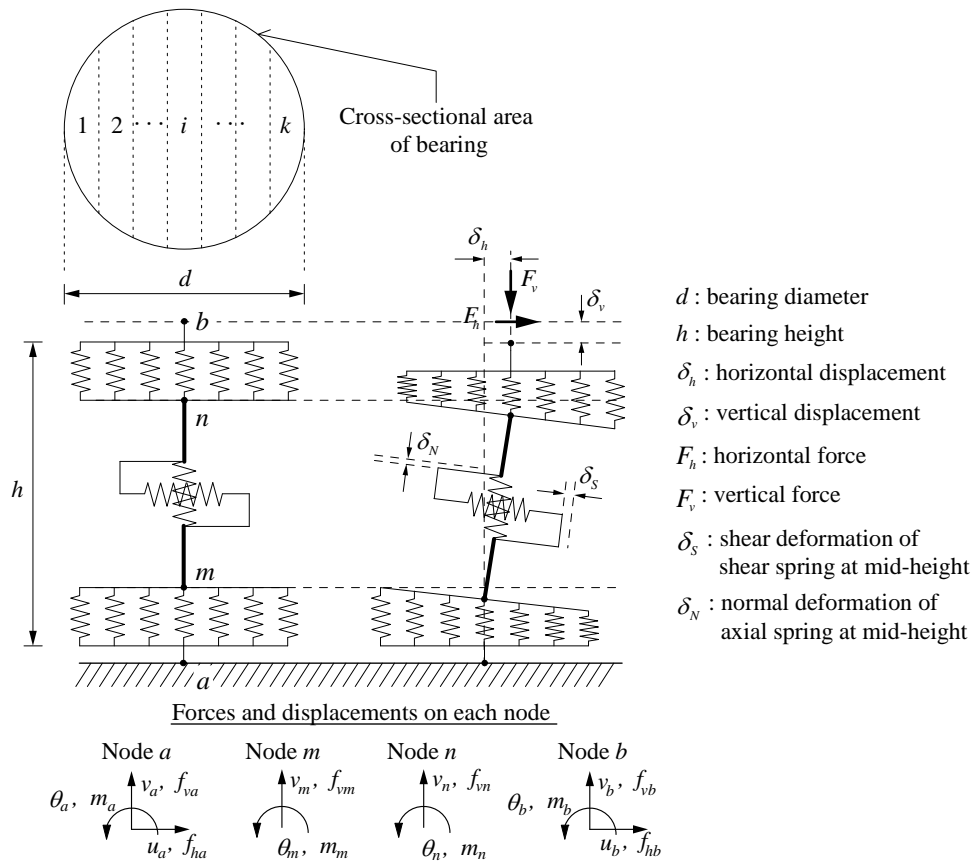


Figure 1 Multi-spring mechanical model

where

$$\begin{aligned}
 {}_1k_{mn} &= K_S + K_N \theta_m^2 \\
 {}_2k_{mn} &= K_S + K_N \theta_n^2 \\
 {}_3k_{mn} &= K_S + K_N \theta_m \theta_n \\
 {}_4k_{mn} &= K_N \theta_m \\
 {}_5k_{mn} &= K_N \theta_n \\
 {}_6k_{mn} &= \frac{hK_S}{2} + \frac{K_N \theta_m (u_b' - u_a')}{2} \\
 {}_7k_{mn} &= \frac{hK_S}{2} + \frac{K_N \theta_n (u_b' - u_a')}{2} \\
 {}_8k_{mn} &= K_N \\
 {}_9k_{mn} &= \frac{K_N (u_b' - u_a')}{2} \\
 {}_{10}k_{mn} &= \frac{h^2 K_S}{4} + \frac{K_N (u_b' - u_a')^2}{4} + K_R \\
 {}_{11}k_{mn} &= \frac{h^2 K_S}{4} + \frac{K_N (u_b' - u_a')^2}{4} - K_R
 \end{aligned}$$

where  $K_S$ ,  $K_N$  and  $K_R$  are the stiffnesses of the mid-height shear, axial and rotational springs, respectively. The rotational spring at the mid-height of the model (which is not shown in Figure 1) is a supplementary element which provides rotational flexibility at the mid-height and gives the new model the ability of handling various distributions of bending moment. The present development assumes that  $K_R$  is infinity. The overall stiffness matrix for an elastomeric bearing,  $\mathbf{K}_{ab}$ , is obtained by arranging the elements of the partial stiffness matrices in Eqn. 2.1 and Eqn. 2.2 into a single  $10 \times 10$  matrix:

$$\begin{Bmatrix} \Delta \mathbf{f}_{ex} \\ \Delta \mathbf{f}_{in} \end{Bmatrix} = \mathbf{K}_{ab} \begin{Bmatrix} \Delta \mathbf{u}_{ex} \\ \Delta \mathbf{u}_{in} \end{Bmatrix} \quad (2.3)$$

where

$$\begin{aligned} \Delta \mathbf{f}_{ex} &= \{ \Delta f_{ha} \quad \Delta f_{va} \quad \Delta m_a \quad \Delta f_{hb} \quad \Delta f_{vb} \quad \Delta m_b \}^T \\ \Delta \mathbf{f}_{in} &= \{ \Delta f_{vm} \quad \Delta m_m \quad \Delta f_{vn} \quad \Delta m_n \}^T \\ \Delta \mathbf{u}_{ex} &= \{ \Delta u_a \quad \Delta v_a \quad \Delta \theta_a \quad \Delta u_b \quad \Delta v_b \quad \Delta \theta_b \}^T \\ \Delta \mathbf{u}_{in} &= \{ \Delta v_m \quad \Delta \theta_m \quad \Delta v_n \quad \Delta \theta_n \}^T \end{aligned}$$

### 3. HYSTERESIS MODELS

In order to predict the large-deformation behavior of elastomeric bearings, nonlinear hysteresis relationships are used for the springs in the new mechanical model. In this section, new hysteresis relationships for the shear and axial springs of the model are developed.

#### 3.1 Shear Spring

Two of the authors previously developed a hysteresis model for the shear deformation of elastomeric isolation bearings that is capable of predicting the behavior of high-damping rubber bearings under large shear deformations [2]. A modification of this earlier model is made to extend its applicability to lead-rubber bearings. Figure 2 (a) shows the modified hysteresis model for the shear deformation of lead-rubber bearings.

#### 3.2 Axial Springs

The new mechanical model has two kinds of axial springs, a series of axial springs at the top and the bottom boundaries, and an axial spring at mid-height. In the present work it is assumed that the series of springs at the top and bottom represent the axial properties of the bearings, and the stiffness of the mid-height axial spring is assumed infinite. Figure 2 (b) shows the stress-strain relationship for the top and bottom series of axial springs.

The stress-strain ( $\sigma$ - $\epsilon$ ) relationship consists of the following four loading states:

(1) Loading and unloading in the elastic region (o-a-b):

$$\sigma = E_{init} \epsilon \quad (3.1)$$

$$E_{init} = \frac{E_0(1 + 2\kappa S_1^2)E_\infty}{E_0(1 + 2\kappa S_1^2) + E_\infty} \quad (3.2)$$

where  $E_0$  is Young's modulus of the rubber,  $\kappa$  is a constant related to rubber hardness,  $S_1$  is the rubber layer shape factor and  $E_\infty$  is the bulk modulus of the rubber.

(2) Loading after tension "yielding" (b-c):

$$\sigma = \sigma_y + E_y(\epsilon - \epsilon_y) \quad (3.3)$$

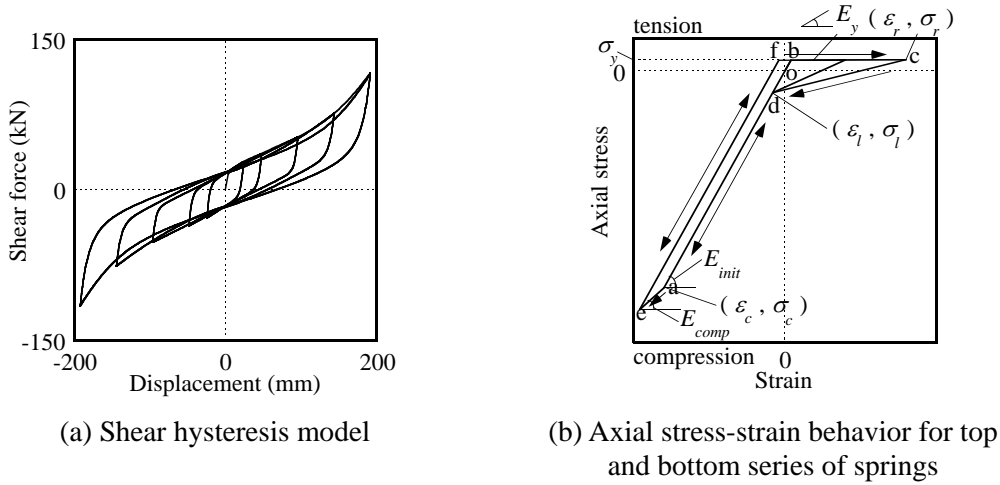


Figure 2 Shear and axial hysteresis models

$$E_y = \frac{1}{500} E_{init} \quad (3.4)$$

$$\sigma_y = E_{init} \varepsilon_y \quad (3.5)$$

where  $\sigma_y$  and  $\varepsilon_y$  are the stress and strain, respectively, of the tension yield point. A value of 1.0 MPa is used for the tension yield stress.

(3) Unloading after tension “yielding” (c-d-a):

$$\sigma = \sigma_r - \frac{\sigma_r - \sigma_l}{\varepsilon_r - \varepsilon_l} (\varepsilon_r - \varepsilon) \quad (\varepsilon_l \leq \varepsilon \leq \varepsilon_r) \quad (3.6)$$

$$\sigma = E_{init} \varepsilon \quad (\varepsilon < \varepsilon_l) \quad (3.7)$$

where  $\sigma_r$  and  $\varepsilon_r$  are the stress and strain of the most recent point of load reversal, and  $\sigma_l$  and  $\varepsilon_l$  are the stress and strain of the target point during unloading after tension yielding.

(4) Loading after compression “yielding” (a-e):

$$\sigma = \sigma_C - E_{comp} (\varepsilon_C - \varepsilon) \quad (3.8)$$

$$E_{comp} = \frac{1}{2} E_{init} \quad (3.9)$$

$$\sigma_C = E_{init} \varepsilon_C \quad (3.10)$$

where  $\sigma_C$  and  $\varepsilon_C$  are the stress and strain, respectively, of the compression yield point. A value of 100 MPa is used for  $\sigma_C$ . When re-loading occurs, even after the compression yield point has been passed, the modulus is still  $E_{init}$ . The stiffness of each axial spring in the series of axial springs,  ${}_i K_{Na}$ , is calculated from Eqn. 3.11:

$${}_i K_{Na} = \frac{{}_i E {}_i A_{div}}{l} \quad (3.11)$$

where  ${}_i E$  is Young’s modulus of each spring in the series of axial springs, which is obtained by referring to the hysteresis model, and  ${}_i A_{div}$  is the area of each divided part.

#### 4. BEARING TESTS AND SIMULATION ANALYSES

Bearing tests were conducted to verify the new analytical model. Two types of cyclic shear tests of lead-rubber bearings were performed. The first were cyclic shear tests with constant vertical loads and the second were cyclic shear tests with varying vertical loads.

##### 4.1 Constant Vertical Load Tests

The bearing tested is shown in Figure 3(a).  $S_2 = 5$  bearing is used for the cyclic shear tests with constant vertical loads. The tests consisted of sinusoidal horizontal displacement-controlled loading, with four fully-reversed cycles of loading at shear strain amplitudes of 50, 100, 200, 300 and 400 %. The loading velocity was 1.5 cm/s. Vertical load on the bearing was maintained constant during each test, and tests were performed at compressive stresses of  $\sigma = 0, 5, 10, 20$  and 30 MPa. The hysteresis loops obtained from the cyclic shear tests of the lead-rubber bearing under constant compressive stresses of 0, 10 and 30 MPa are shown in Figure 4. The bearing exhibited obvious shear stiffening behavior beyond approximately 300 % shear strain at low axial stresses of 0 and 10 MPa. However, the bearing exhibited significant negative stiffness for a stress of 30 MPa. The results show that compressive stress strongly influences the shear hysteretic behavior of the lead-rubber bearing design tested.

Simulation analyses of the tests were conducted to validate the proposed mechanical model and the spring hysteresis models. The following material properties were used for the analyses: Young's modulus of rubber,  $E_0 = 1.44$  MPa, bulk modulus of rubber,  $E_\infty = 1960$  MPa, and the constant related to rubber hardness,  $\kappa = 0.85$ . Figure 5 shows the hysteresis loops predicted by the analytical model for the same loading histories and compressive stress as the experimental hysteresis loops shown in Figure 4. Comparing Figures 4 and 5, the experimental and analytical results show good agreement under all three levels of compressive stress. The results show that the proposed model can accurately predict complex nonlinear behaviors for lead-rubber bearings under large deformations, as a function of the imposed axial stress on bearing.

##### 4.2 Varying Vertical Load Tests

An advantage of the proposed model is its capability to predict a variety of force-displacement relationships for an isolation bearing with a single model of the bearing. To confirm this capability, cyclic shear tests of lead-rubber bearings under varying vertical load were conducted. The bearings tested are shown in Figure 3. Two types of bearing,  $S_2 = 5$  bearing and  $S_2 = 4$  bearing, were used for the cyclic shear tests with varying vertical loads. The tests of the  $S_2 = 5$  bearing comprised cyclic shear tests with the vertical load varying (during shear cycling) between 0 and 30 MPa, and the tests of the  $S_2 = 4$  bearing comprised cyclic shear tests with the vertical load varying (during shear cycling) between 0 and 20 MPa. The shear and axial loading histories for

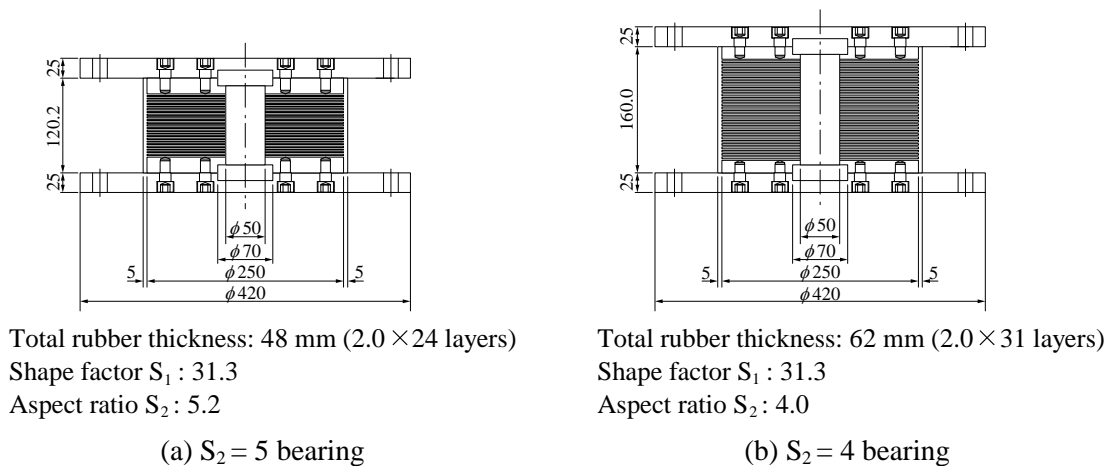


Figure 3 Lead-rubber bearing designs tested

both bearing types are shown in Figure 6. The hysteresis loops obtained from the tests are shown in Figure 7. These loops are not symmetric, rather they show both shear stiffening behavior and a deterioration of horizontal stiffness depending upon the level of vertical load on the bearing.

Figure 8 shows the hysteresis loops predicted by the analytical model for the same shear and axial loading histories as the experimental hysteresis loops shown in Figure 7. The analytical results for both the  $S_2 = 5$  and 4 bearings show very good agreement with the experimental results (Figure 7). This agreement demonstrates that the proposed model can accurately predict the influence of varying vertical loads on these types of elastomeric isolation bearings.

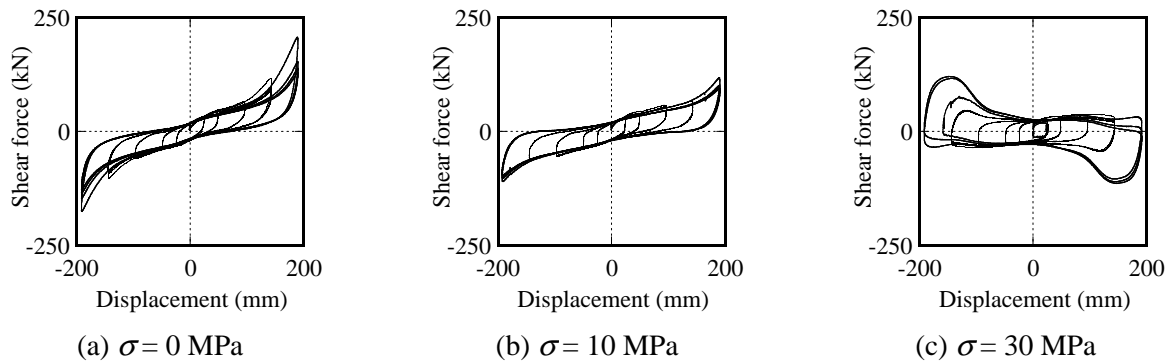


Figure 4 Experimental shear hysteresis loops for cyclic shear tests of lead-rubber bearing ( $S_2 = 5$ ) with constant vertical loads

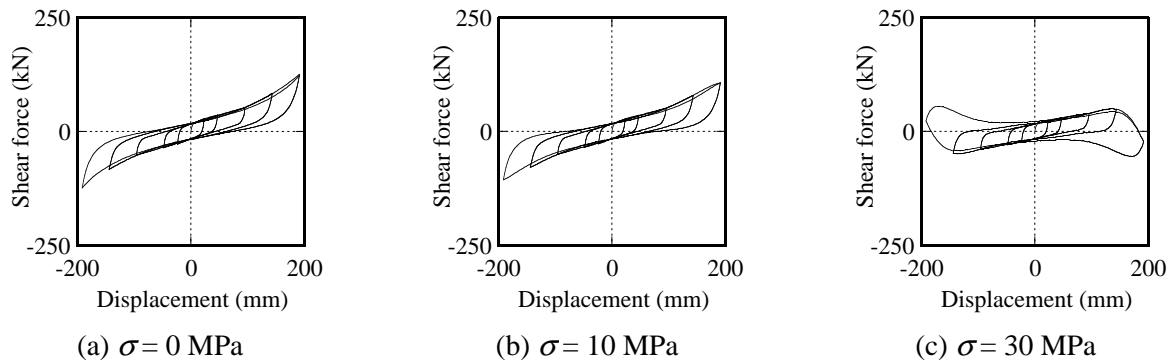


Figure 5 Analytical shear hysteresis loops for lead-rubber bearing cyclic shear loading with constant vertical loads

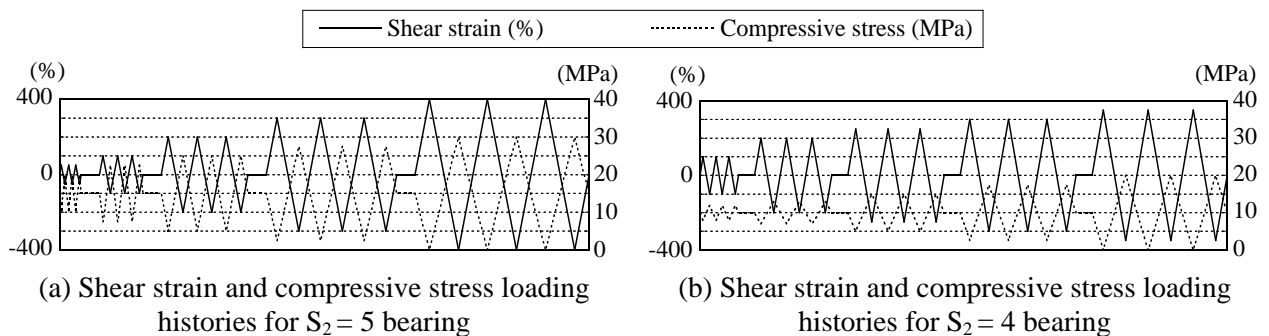


Figure 6 Loading histories for combined shear and varying vertical load tests

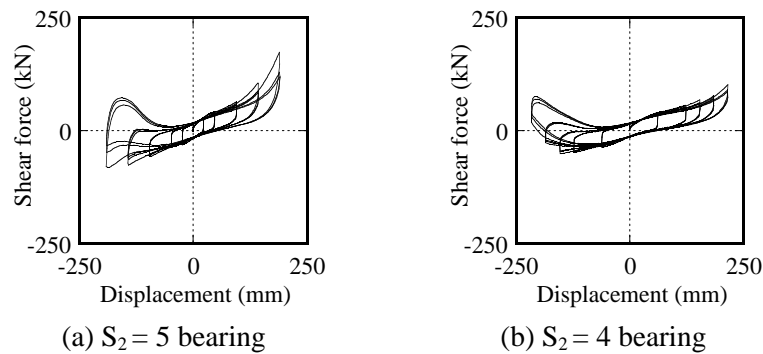


Figure 7 Experimental shear hysteresis loops for lead-rubber bearing cyclic shear tests with varying vertical loads

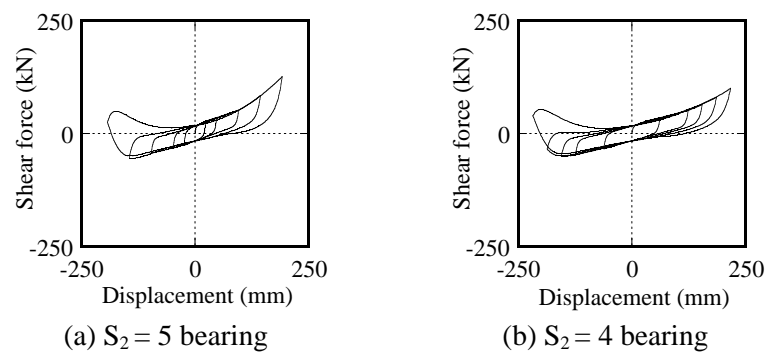


Figure 8 Analytical shear hysteresis loops for lead-rubber bearing cyclic shear loading with varying vertical loads

## 5. CONCLUSIONS

A new analytical model for elastomeric seismic isolation bearings is proposed to more accurately predict the large displacement response of isolated buildings. The proposed model includes the interaction between shear and axial forces, nonlinear hysteresis and dependence on varying vertical load. The hysteresis models for the shear spring and the series of axial springs in the new model were developed separately to appropriately represent the large deformation behaviors of elastomeric bearings. Cyclic shear tests of a lead-rubber bearing under constant vertical load were performed as part of the development of the new model. The lead-rubber bearing tested exhibited stiffening or buckling behavior influenced by axial stress under large deformations. Through comparison with the test results, the new model is shown to successfully predict a variety of complex bearing force-displacement relationships under a wide range of vertical load conditions. Cyclic shear tests under varying vertical load were performed to assess the influence of varying vertical load on bearing hysteretic behavior. The hysteresis loops obtained from the tests were not symmetric and showed both stiffening and deteriorating shear stiffness, due to the varying vertical load. The analytical results given by the new model show very good agreement with actual bearing test results. The capabilities that have been demonstrated for the new model make it a useful tool for the more accurate dynamic analysis in which it is desired to include the effect of varying vertical load on isolation bearings during severe earthquake loading.

## REFERENCES

1. Kelly, J.M. (1997). *Earthquake-Resistant Design with Rubber* (2nd edition), Springer, London.
2. Kikuchi, M. and Aiken, I.D. (1997). An analytical hysteresis model for elastomeric seismic isolation bearings. *Earthquake Engineering and Structural Dynamics* **26**, 215-231.